Abdominal Radiology

Published online: 4 September 2018

Abdom Radiol (2019) 44:576–585
https://doi.org/10.1007/s00261-018-1763-1

Textural analysis on contrast-enhanced CT in pancreatic neuroendocrine neoplasms: association with WHO grade

Chuangen Guo,[1] Xiaoling Zhuge,[2] Zhongqiu Wang,[3] Qidong Wang,[1] Ke Sun,[4] Zhan Feng,[1] and Xiao Chen[3]

[1]Department of Radiology, The First Affiliated Hospital, College of Medicine, Zhejiang University, 79 Qingchun Road, Hangzhou 310003, China
[2]Department of Laboratory Medicine, The First Affiliated Hospital, College of Medicine, Zhejiang University, 79 Qingchun Road, Hangzhou 310003, China
[3]Department of Radiology, The Affiliated Hospital of Nanjing University of Chinese Medicine, 155 Hanzhong Road, Nanjing 2100029, China
[4]Department of Pathology, College of Medicine, The First Affiliated Hospital, Zhejiang University, 79 Qingchun Road, Hangzhou 310003, China

Abstract

Purpose: Grades of pancreatic neuroendocrine neoplasms (PNENs) are associated with the choice of treatment strategies. Texture analysis has been used in tumor diagnosis and staging evaluation. In this study, we aim to evaluate the potential ability of texture parameters in differentiation of PNENs grades.
Materials and methods: 37 patients with histologically proven PNENs and underwent pretreatment dynamic contrast-enhanced computed tomography examinations were retrospectively analyzed. Imaging features and texture features at contrast-enhanced images were evaluated. Receiver operating characteristic curves were used to determine the cut-off values and the sensitivity and specificity of prediction.
Results: There were significant differences in tumor margin, pancreatic duct dilatation, lymph nodes invasion, size, portal enhancement ratio (PER), arterial enhancement ratio (AER), mean grey-level intensity, kurtosis, entropy, and uniformity among G1, G2, and pancreatic neuroendocrine carcinoma (PNEC) G3 ($p < 0.01$). Similar results were found between pancreatic neuroendocrine tumors (PNETs) G1/G2 and PNEC G3. AER and PER showed the best sensitivity (0.86–0.94) and specificity (0.92–1.0) for differentiating PNEC G3 from PNETs G1/G2. Mean grey-level intensity, entropy, and uniformity also showed acceptable sensitivity (0.73–0.91) and specificity (0.85–1.0). Mean grey-level intensity was also showed acceptable sensitivity (91% to 100%) and specificity (82% to 91%) in differentiating PNET G1 from PNET G2.
Conclusions: Our data indicated that texture parameters have potential in grading PNENs, in particular in differentiating PNEC G3 from PNETs G1/G2.

Key words: Pancreatic neuroendocrine neoplasms—Grade—Pancreatic neuroendocrine carcinoma—Texture analysis—Computed tomography

Pancreatic neuroendocrine neoplasms (PNENs) are rare diseases of pancreas, which account 1% to 2% of all pancreatic neoplasms [1]. Recent studies have shown that the incidence of NENs has increased to 6.98 per 100,000 per year (3.56 per 100,000 in gastroenteropancreas) in general population [2]. PNENs show multiple biological behaviors. However, all PNENs have malignant potential. The PNENs are divided into pancreatic neuroendocrine tumors (PNETs) grade 1 (G1), PNET G2, and neuroendocrine carcinoma (PNEC) G3 based

Chuangen Guo and Xiaoling Zhuge have contributed equally to this work.

Correspondence to: Zhan Feng; *email:* gerxyuan@zju.edu.cn; Xiao Chen; *email:* chxwin@163.com

on the mitotic count and the Ki-67 proliferation index in WHO 2010 classification of tumors of the digestive system [3].

The treatment strategies and prognosis of PNENs are related with the tumor grade. For PNETs G1/G2, surgical resection is usually adopted, in particular to those tumors without local invasion or distal metastases [4]. In addition, targeted therapies with everolimus or sunitinib and somatostatin analogs (octreotide) are also valuable for PNETs G1/G2 [5–7]. For PNEC G3, chemotherapy or radiotherapy is usually used besides surgical resection [4]. The grades of PNENs are depended on histological examinations. The pretreatment predication of PNENs grade is valuable for surgeons in determining treatment strategies. Recently, dynamic contrast-enhanced computed tomography (CT) [8–11] and magnetic resonance imaging (MRI) [12, 13] are available in differentiating PNETs G1/G2 from PNEC G3. CT features, such as arterial enhancement ratio (AER) and portal enhancement ratio (PER), and diffusion-weighted magnetic resonance imaging (MRI) can be used to differentiate PNEC G3 from PNETs G1/G2. PNEC G3 usually shows lower AER, PER, and apparent diffusion coefficients (ADCs) values than PNETs G1/G2.

Recently, texture analysis has been widely used in radiologic field. Texture analysis evaluates the characterization of regions of interest (ROIs) in an image by analyzing the variation in pixel intensities [14]. Texture analysis can provide important information concerning tumor physiology [15–17]. More and more studies indicated that texture analysis could be used for tumor detection, diagnosis, staging, evaluation of treatment response, and prognosis [14, 18–22]. Usually, texture parameters include two orders: first order (energy, entropy, skewness) and second order (grey level and run length co-occurrence matrix) [14]. Hundreds of parameters can be extracted from one image [22]. Pereira et al. [23] indicated that histogram analysis on apparent diffusion coefficient (ADC) maps was correlated with PNENs histological grade. However, the population sizes were relatively small, in particular to PNET G2 ($n = 4$) and PNEC G3 ($n = 3$). We speculated that it might be a potential approach for PNENs grading. To the best of our knowledge, few studies investigate the role of texture analysis on contrast-enhanced CT in grading PNENs [24, 25]. However, the number of PNEC G3 is small in those studies ($n = 3$–5).

In the present study, we aimed to show the differences in texture parameters, including entropy, skewness, kurtosis, uniformity, and mean grey-level intensity, among PNET G1, PNET G2, and PNEC G3. Effort was also made to show the differences in texture parameters between PNETs G1/G2 and PNEC G3. In addition, the routine imaging findings also were reviewed.

Material and methods

This retrospective study was approved by the Institutional Review Board of the First Affiliated Hospital, College of Medicine Zhejiang University. For this retrospective study, the requirement of the formal consent was waived.

Patients' selection

From January 2013 to May 2016, we identified 72 patients with surgically proven PNENs in our hospital's data warehouse. The following criteria were used for patients' inclusion: (1) patients with pathology-proven PNENs; (2) patients underwent dynamic pancreas CT within 30 days prior to surgery or biopsy; (3) the patients did not receive chemotherapy or local treatments before surgery; and (4) primary PNENs. 35 patients were excluded as the following reasons: CT data absent ($n = 24$), only received CT angiography ($n = 3$) or non-contrast CT examinations ($n = 4$), and metastatic PNENs ($n = 4$). Finally, total of 37 patients were included in this study (Fig. 1).

CT protocol

All CT imaging was performed on multidetector CT system (BriBrillianceiCT, Philips, The Netherland) according to a standardized protocol. Patients fasted for 8 h prior to CT examination. All scans were performed in the head-first supine position. Non-enhanced, arterial, and portal venous phase images were obtained from each patient. The imaging parameters were as following: tube

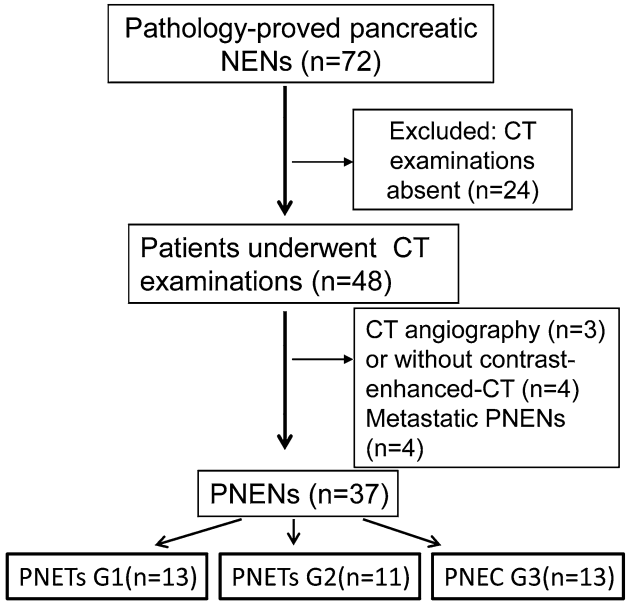

Fig. 1. Flow diagram of the study patients with pancreatic neuroendocrine neoplasms (PNENs).

voltage, 120 kV; slice thickness, 3 mm; slice interval, 1 mm; beam collimation, 0.625 mm × 128; beam pitch, 0.91; and tube current, automatic tube current modulation. For contrast-enhanced CT scan, ultravist (300 mg/mL, Bayer HealthCare Pharmaceuticals, Germany) was administered at a dose of 1.5 mL/kg (3.0 mL/s). Bolus tracking technique was used to trigger the arterial phase scan. The enhanced images were obtained at arterial phase (30–35 s) and portal phase (55–60 s). The slice thickness of reconstruction was set at 2.0 mm for diagnostic reading.

Image analysis

The images were analyzed by two abdominal radiologists with more than 6 years of clinical experience in abdominal CT reading. They knew the presence of PNENs, but they were blinded to pathologic grade. The following imaging parameters were reviewed: tumor location, size, tumor margin (well-circumscribed or ill-defined border), components (solid or cystic-solid), calcification, tumor attenuation on unenhanced CT scan, enhancement degree (low to moderate: increase of CT values < 20 HU; marked enhanced increase of CT values > 20 HU), arterial enhancement ratio (AER: HU values of tumor/HU values of normal parenchyma measured on arterial phase), portal enhancement ratio (PER: HU values of tumor/HU values of normal parenchyma measured on portal phase), vascular invasion, and the presence of pancreatic duct dilatation and metastases (lymph node, local invasion, or distal metastases). Cystic components of the tumor were identified as areas that were not enhanced at both arterial phase and venous phase. The regions of interest (ROIs) for CT values measurement were manually drawn on the solid components. The definition of tumor margin and tissue components was referenced from the previous study [9]. Briefly, solid was regarded as if enhancing tissues $> 90\%$; well-circumscribed was defined as smooth margin without spiculation or with less than 80% of infiltration; pancreatic duct dilatation was regarded as the main pancreatic duct diameter ≥ 4 mm.

Texture analysis

Because the tumor showed the highest resolution at arterial phase, the images at arterial phase were used for texture analysis. ROIs were manually drawn in consensus by two abdominal radiologists in Matlab 2014 (> 6 years of clinical experience in abdominal CT). The ROIs were the largest size within solid tissues. Texture analysis was performed by using Matlab 2014a (MathWorks, Natick, MA) by one of the abdominal radiologists (3 years of experience in Matlab) (Fig. 2). Necrotic components were excluded from ROIs. Texture analysis was performed at five slices of each tumor, including the largest cross-sectional slice and the following two continues slices at upper and low cross-sections. The CT texture parameters were obtained using the filtration-histogram approach as the previous reports [26, 27]. Laplacian of Gaussian band-pass filters (filter sigma values of 0.5, 1.5, and 2.5) were used as suggested in previous study [28, 29]. In order to reduce the impact of non-target regions, we set the regions outside the ROI with the average value of the pixels inside the ROI [29]. The texture parameters included mean grey-level intensity, kurtosis, skewness, entropy, and uniformity which had been used in previous reports [26, 28, 29]. The mean of each parameter was calculated automatically. The mathematical expression and means of texture parameters were reported in the previous study [26]. The inter-observer agreements in ROIs were assessed with Conger's kappa test. For those cases with interobserver disagreement, texture analysis was not performed until the two readers reach a consensus.

Histological analysis

The histological analysis was performed as described in our previous study [13]. Briefly, the tumor specimens were fixed with 10% formalin solution for 12 h, dehydrated with series ethanol (40% to 100%), embedded in paraffin, sliced with a microtome, and then the sections were stained with hematoxylin-eosin (H&E) and immunohistochemical analysis. The number of mitosis

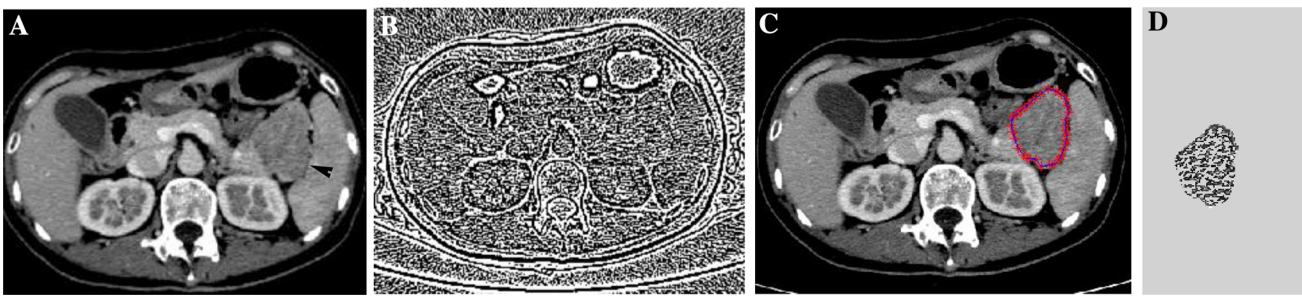

Fig. 2. The regions of interest (ROIs) placement and tumor segmentation. **A** Pancreatic neuroendocrine carcinoma in CT image (arrow head). **B** Filtered images at sigma value of 1.5. **C** ROI drawn on an axial image with the largest cross-sectional area of the tumor (red line). **D** The tumor segmentation.

[per 10 high-power fields (HPF)] and Ki-67 proliferation index (percentage of positive cells in areas of highest nuclear labeling) were calculated. The PNENs were classified as PNET G1, PNET G2, and PNEC G3 according to the WHO 2010 classification for neuroendocrine tumors: NET G1: < 2 mitoses per 10 HPF, Ki-67 ≤ 2%; NET G2: 2–20 mitoses per 10 HPF, Ki-67 index 3% to 20%; and PNEC G3: > 20 mitoses per 10 HPF, Ki-67 index > 20%.

Statistical analysis

The data were managed and analyzed by using SPSS 16.0 (SPSS Inc, Chicago, IL). Quantitative data were displayed as means ± SD or median and were analyzed by Kruskal–Wallis H test or one-way analysis of variance (ANOVA). Qualitative data were expressed as number and were analyzed using the Chi-square test or Fisher's exact test. Spearman rank correlation was performed to show the association between texture parameters and histopathologic variables. The cut-off values and the sensitivity and specificity of prediction were calculated by using Receiver operating characteristic (ROC) curves by using MedCalc software (Mariakerke, Belgium). p value < 0.05 was considered as statistically significant.

Results

Patients' characteristics

The characteristics of the patients are displayed in Table 1. PNETs G1 and PNEC were both observed in thirteen patients. PNET G2 was found in eleven patients. Five cases underwent biopsy (Four in PNETs and one in PNEC). No significant differences were found in age and tumor location among PNET G1, G2, and PNEC G3. Significant differences were observed in clinical symptoms and in gender among G1, G2, and G3 tumors ($p < 0.05$). We also compared the clinical data between PNETs G1/G2 and PNEC G3. Our data showed that PNETs G1 and G2 were usually asymptomatic ($p < 0.05$), while abdominal pain usually occurred in PNEC G3 ($p < 0.05$). There were no significant differences between PNET G1 and G2.

CT imaging findings

The CT imaging findings are summarized in Table 2. Significant differences were found in tumor margin, enhancement degree (arterial and portal phase), pancreatic duct dilatation, lymph nodes invasion, local invasion/vascular invasion or metastases, size (cm), PER, and AER among PNETs G1, G2, and PNEC G3 tumors (all $p < 0.05$ or 0.01). Similar results were found between PNETs G1/G2 and PNEC G3. PNEC G3 usually showed ill-defined margin, low-moderate enhancement, pancreatic duct dilatation, lymph nodes invasion, local invasion/vascular invasion or metastases, and larger sizes compared with PNETs G1/G2 (all $p < 0.05$ or 0.01). In addition, the AER and PER in PNEC G3 were significantly lower than PNETs G1/G2 ($p < 0.01$). No significant differences were found in CT imaging findings between PNET G1 and G2 except for tumor size.

CT texture parameters

The Kappa value was 0.81 for ROIs drawing. The CT texture parameters among G1, G2, and G3 tumors were summarized in Table 3. Significant differences were found in mean grey-level intensity regardless of the size of filters among G1, G2, and G3 tumors ($p < 0.01$). However, for kurtosis, entropy, and uniformity, no significant differences were found among G1, G2, and G3 at low sigma value (0.5). Significant differences were observed at moderate and high sigma values ($p < 0.01$). Similar results were found between PNETs G1/G2 and PNEC G3. No differences were found among G1, G2, and G3 tumors or between G1/G2 and G3 in skewness. Significant differences were found in mean grey-level

Table 1. Clinical data of patients

Variables	PNET G1 (n = 13)	PNET G2 (n = 11)	PNEC G3 (n = 13)	p	p*
Age (years)	54.9 ± 8.2 (41–61)	54.3 ± 11.4 (28–74)	53.9 ± 13.1 (25–70)	> 0.05	> 0.05
Gender				< 0.01	< 0.01
Male	7	2	11		
Female	6	9	2		
Clinical symptoms					
Abdominal pain	3	3	9	0.03	0.02
Weakness	3	0	1		
Yellow urine or icterus	0	0	1		
Asymptomatic	7	8	2	0.02	0.016
Location				> 0.05	> 0.05
Pancreatic head–neck	6	5	6		
Pancreatic body–tail	7	6	7		

PNET G1, pancreatic neuroendocrine tumor grade 1; PNEC, pancreatic neuroendocrine carcinoma
p*: G3 vs G1/G2

Table 2. The summary of CT findings

CT findings	Tumor grade			p	p*
	PNET G1 (n = 13)	PNET G2 (n = 11)	PNEC G3 (n = 13)		
Margin				< 0.05	< 0.05
Well-circumscribed	12	10	7		
Ill-defined	1	1	6		
Solid and cystic pattern				0.15	0.11
Predominant solid	11	9	7		
Cystic-solid	2	2	6		
Enhancement degree (arterial phase)				< 0.001	< 0.01
Marked enhancement	12	8	4		
Low to moderate enhancement	1	3	9		
Enhancement degree (portal phase)				< 0.001	< 0.001
Marked enhancement	12	9	4		
Low to moderate enhancement	1	2	9		
Pancreatic duct dilatation	1	1	7	< 0.05	< 0.05
Pancreatic atrophy	1	1	3	< 0.05	< 0.05
Lymph nodes invasion	0	2	8	< 0.01	< 0.01
Local invasion, vascular invasion, or metastases	0	1	6	< 0.05	0.01
Size (cm)[#]	1.7 ± 0.9	3.5 ± 1.6	5.0 ± 4.2	< 0.01	< 0.01
Arterial enhancement ratio	1.7 ± 0.3	1.5 ± 0.4	0.8 ± 0.2	< 0.01	< 0.01
Portal enhancement ratio	1.3 ± 0.1	1.1 ± 0.2	0.76 ± 0.1	< 0.01	< 0.01

PNET, pancreatic neuroendocrine tumor; PNEC, pancreatic neuroendocrine carcinoma
p*: G3 vs G1/G2
[#]$p < 0.05$, G1 vs. G2

Table 3. The summary of CT texture parameters

Texture index	Sigma value (σ)	PNET G1 (n = 13)	PNET G2 (n = 11)	PNEC G3 (n = 13)	p	p*
Mean grey-level intensity	0.5[#]	− 0.99 ± 0.50 (− 0.84)	− 0.28 ± 0.26 (− 0.21)	− 0.07 ± 0.07 (− 0.07)	< 0.01	< 0.01
	1.5[#]	− 1.33 ± 0.60 (− 1.09)	− 0.42 ± 0.37 (− 0.32)	− 0.10 ± 0.08 (− 0.08)	< 0.01	< 0.01
	2.5[#]	− 1.44 ± 0.57 (− 1.25)	− 0.50 ± 0.43 (− 0.38)	− 0.12 ± 0.09 (− 0.08)	< 0.01	< 0.01
Kurtosis	0.5	3.67 ± 0.54 (3.54)	5.4 ± 2.84 (3.88)	3.98 ± 1.56 (3.40)	0.74	0.59
	1.5[#]	4.52 ± 1.18 (4.39)	18.0 ± 27.9 (5.31)	10.65 ± 11.27 (6.75)	0.02	0.04
	2.5[#]	3.86 ± 0.65 (3.65)	18.6 ± 34.8 (5.66)	13.11 ± 9.87 (10.73)	< 0.01	< 0.01
Skewness	0.5	− 0.12 ± 0.13 (− 0.13)	− 0.13 ± 0.34 (− 0.12)	− 0.10 ± 0.19 (− 0.06)	0.57	0.36
	1.5	− 0.55 ± 0.49 (− 0.38)	− 0.94 ± 1.27 (− 0.48)	− 0.56 ± 1.12 (− 0.47)	0.72	0.45
	2.5	− 0.66 ± 0.52 (− 0.68)	− 1.37 ± 1.79 (− 0.86)	− 0.82 ± 1.17 (− 0.85)	0.75	0.76
Entropy	0.5	4.95 ± 0.56 (4.92)	4.70 ± 0.53 (4.65)	4.47 ± 0.50 (4.50)	0.135	0.07
	1.5	3.65 ± 0.40 (3.63)	3.37 ± 0.55 (3.29)	2.74 ± 0.43 (2.62)	< 0.01	< 0.01
	2.5	3.06 ± 0.31 (3.04)	2.75 ± 0.61 (2.50)	1.95 ± 0.36 (1.84)	< 0.01	< 0.01
Uniformity	0.5	0.04 ± 0.015 (0.04)	0.05 ± 0.019 (0.05)	0.06 ± 0.033 (0.05)	0.15	0.07
	1.5	0.10 ± 0.028 (0.10)	0.13 ± 0.05 (0.13)	0.19 ± 0.085 (0.21)	< 0.01	< 0.01
	2.5	0.15 ± 0.033 (0.15)	0.21 ± 0.058 (0.23)	0.35 ± 0.088 (0.37)	< 0.01	< 0.01

PNET, pancreatic neuroendocrine tumor; PNEC, pancreatic neuroendocrine carcinoma
Data were shown as mean ± SD (median)
p*: G3 vs. G1/G2
[#]G1 vs. G2, $p < 0.05$ or 0.01

intensity and kurtosis (high sigma values) between PNET G1 and G2 ($p < 0.05$ or 0.01).

Correlation analysis

Spearman correlation analysis between tumor pathological data (grade and Ki-67 index) and imaging findings, and texture parameters is shown in Fig. 3. Firstly, we evaluated the correlation between tumor pathological data and CT imaging findings. Tumor grade (G1, G2, G3 and G1/G2, G3) was positively correlated with, lymph nodes invasion, local invasion/vascular invasion/metastasis, and negatively correlated with AER, PER, and tumor margin (all $p < 0.01$). We also observed the association between tumor pathological data and CT texture parameters. Tumor grade (three grades, G1, G2, and G3; 2 grades, G1/G2 and G3) was positively correlated with mean grey-level intensity (at all sigma values), kurtosis (at moderate and high sigma values), uniformity (at moderate and high sigma values), and negatively correlated with entropy (all $p < 0.05$). Similar results were found in the association between Ki-67 index and imaging findings or texture parameters. Mean grey-level intensities (at all sigma values) were also positively

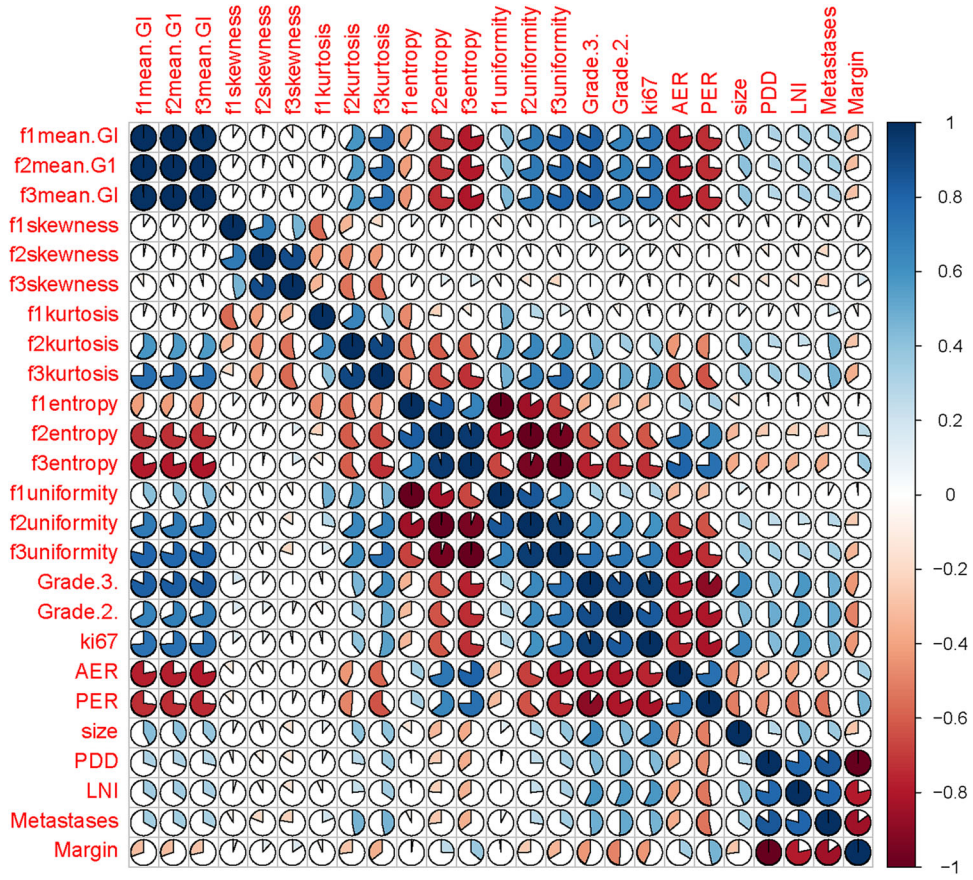

Fig. 3. The correlation between CT imaging findings, texture parameters, and tumor histological grade. GI: grey-level intensity; PDD, pancreatic duct dilatation; LNI, lymph nodes invasion. f1–f3 mean sigma values of 0.5, 1.5, and 2.5, respectively.

($p < 0.001$) correlated and kurtosis (at high sigma values) was negatively correlated ($p < 0.05$) with tumor grades in PNET G1/G2.

Diagnostic performances of imaging findings and texture parameters

The sensitivity and specificity of the different imaging features and texture parameters for PNEC G3 identification (vs. PNETs G1/G2) ranged from 45% to 94% and 85% to 100%, respectively (Table 4). The area under the curve (AUC) ranged from 71% to 98% (Table 4). AER, PER, mean grey-level intensity (at all sigma values), entropy (at high sigma values), and uniformity (at high sigma values) had the largest AUC (≥ 0.90). Cut-off values were 1.06 for AER with 94% sensitivity and 92% specificity, 0.92 for PER with 86% sensitivity and 100% specificity, 2.4 for entropy (at high sigma values) with 91% sensitivity and 85% specificity, and 0.21 for uniformity (at high sigma values) with 73% sensitivity and 100% specificity. For mean grey-level intensity at three sigma values, the cut-off values were 0.20, 0.30, and 0.36, with 82% sensitivity and 92% to 100% specificity, respectively. We also showed the sensitivity and specificity of the sizes, AER, PER, and mean grey-level intensity for differentiating PNET G1 from PNET G2 (Fig. 4). Size and mean grey-level intensity showed the largest AUC. The AUC, sensitivity, and specificity ranged from 0.88 to 0.94, 91% to 100%, and 82% to 91%, respectively.

Subsequently, we analyzed the diagnostic performances of imaging findings (sizes and margin) and texture parameters (f3 mean grey-level intensity and f3 entropy) by using a multivariate model (Table 5). The AUC for imaging features, texture features, and sizes/margin + texture features were 0.802 (100% sensitivity and 55.0% specificity), 0.936 (91.7% sensitivity and 84.6% specificity), and 0.958 (91.6% sensitivity and 87.5% specificity).

Discussion

The histological grade of PNENs is marked related with the therapeutic management and the prognosis. Several studies have shown that imaging approaches, such as DCE-CT and DWI-MRI, are valuable for PNENs identification [8, 9, 12], especially for the differentiation between PNEC G3 and PNETs G1/G2. In the present study, we showed the differences in imaging findings and

Table 4. Diagnostic performances of imaging features and texture parameters for differentiating PNEC G3 from PNETs G1/G2

Variables	AUC	Sensitivity (%) (95% CI)	Specificity (%) (95% CI)	Cut-off point
AER	0.98	94 (77–100)	92 (64–100)	1.06
PER	0.98	86 (65–97)	100 (75–100)	0.92
f1 mean grey-level intensity	0.90	82 (60–95)	92 (64–100)	0.20
f2 mean grey-level intensity	0.91	82 (60–95)	100 (75–100)	0.30
f3 mean grey-level intensity	0.92	82 (59–95)	100 (75–100)	0.36
f2 kurtosis	0.71	59 (36–79)	92 (64–100)	4.65
f3 kurtosis	0.80	77 (55–92)	85 (55–98)	0.57
f2 uniformity	0.87	63 (41–83)	100 (75–100)	0.11
f3 uniformity	0.93	73 (50–89)	100 (75–100)	0.21
f2 entropy	0.87	63 (41–83)	100 (75–100)	3.4
f3 entropy	0.94	91 (71–99)	85 (55–98)	2.4
Sizes	0.77	45 (24–68)	100 (75–100)	1.8
Pancreatic duct dilatation	0.72			
Lymph nodes invasion	0.76			
Local invasion or metastases	0.71			
Margin	0.72			

f1–f3 means sigma values of 0.5, 1.5, and 2.5, respectively
PNET, pancreatic neuroendocrine tumor; PNEC, pancreatic neuroendocrine carcinoma; AUC, area under the curve; CI, confidence interval

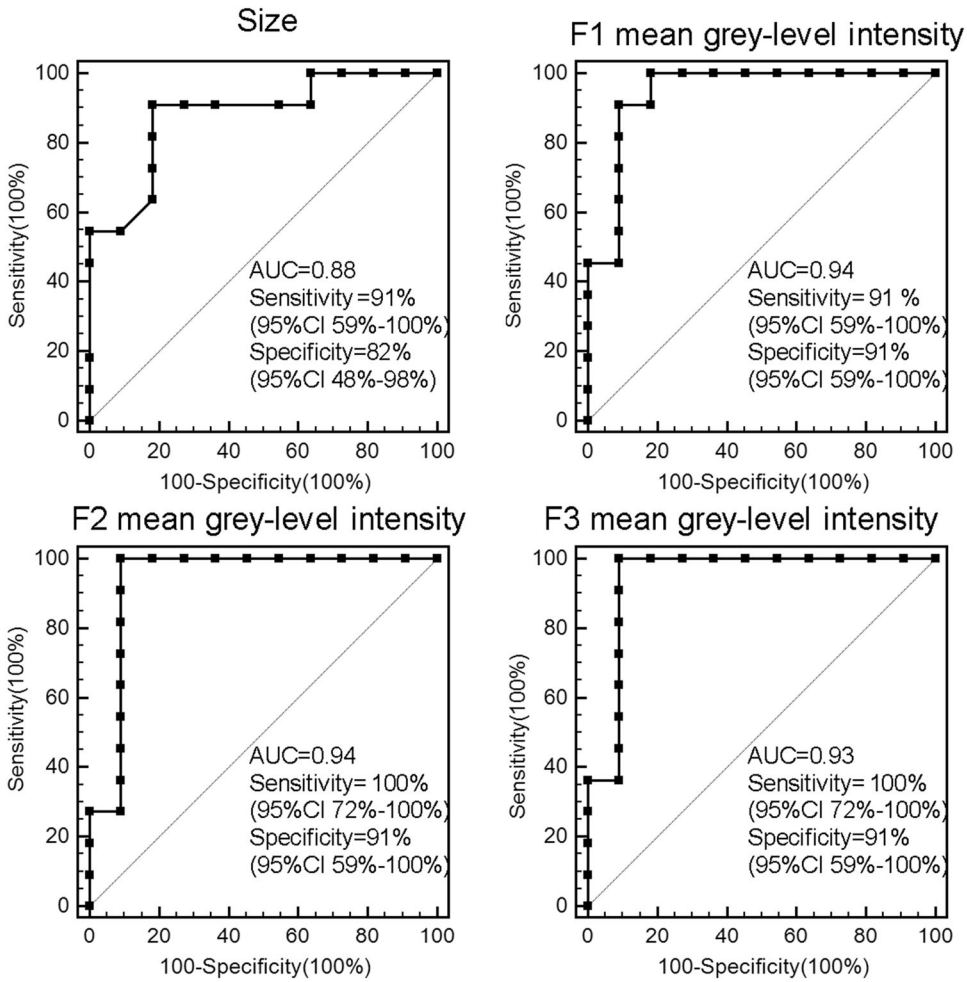

Fig. 4. Receiver operating characteristic (ROC) curve of tumor size and mean grey-level intensity for differentiating PNET G1 from PNET G2. f1–f3 mean sigma values of 0.5, 1.5, and 2.5, respectively.

Table 5. Multivariate logistic regression models for differentiating PNEC from PNETs G1/G2 on imaging features and CT texture features

	Sensitivity (%) (95% CI)	Specificity (%) (95% CI)	AUC
Imaging features	100 (73.5–100)	55.0 (31.5–76.9)	0.802
Texture features	91.7 (61.5–99.8)	84.6 (54.6–98.1)	0.936
Sizes/margin + texture features	91.6 (61.5–99.8)	87.5 (47.38–99.7)	0.958

Imaging features include sizes and margin; texture features include f3 mean grey-level intensity and f3 entropy
CI, confidence interval; AUC, area under the curve

texture parameters among G1, G2, and G3 tumors. Our data indicated that there were significant differences in AER, PER, margin, pancreatic duct dilatation, lymph nodes invasion, mean grey-level intensity, entropy, uniformity, and kurtosis among G1, G2, and G3 tumors. Moreover, our data further showed that those parameters above were also valuable in the differentiation of PNEC G3 from PNETs G1/G2 tumors.

Effort has been made to differentiate PNEC G3 from PNETs G1/G2 by using contrast-enhanced CT [9, 11]. Several studies showed that vascular invasion and large size were more common in PNEC G3 compared with PNETs G1/G2 [9, 24]. In addition, Kim et al. also found that the AER and PER of PNEC G3 were significantly lower than those of PNETs G1/G2 [9]. PER < 1.1 showed the 92.3% sensitivity and 80.5% specificity. Horiguchi et al. showed that AER of PNEC G3 was significantly lower than that of PNETs G1/G2 (0.5 vs. 1.5). Our study also showed that ill-defined margin, lymph node invasion, local invasion/vascular invasion/metastases, and larger sizes were more common found in PNEC G3 than PNETs G1/G2, which were consistent with the previous report [9, 24]. AER value in our study was closed to those previous reports. Our data were also consistent with the previous findings that AER and PER could be used for the differentiation between PNEC G3 and PNETs G1/G2 [9, 11]. However, there are mild differences because different statistical analyses were used. The cut-off in our study was calculated by ROC with the highest sensitivity + specificity. The previous study divided the AER and PER into two subgroups [9], then calculated the sensitivity and specificity. In addition, there are mild differences in acquisition time of images which may affect the AER and PER values. In our series, no significant differences in imaging findings were found between PNET G1 and PNET G2 except for tumor size. Takumi et al. [10] also compared the imaging findings on contrast-enhanced CT between PNET G1 and PNET G2. They observed that the contrast-enhanced degree of PNET G2 was lower than PNET G1, in particular at portal phase. Similar trends were also observed in our study, but no significant differences were found ($p = 0.069$ at portal phase). We speculated that this phenomenon may be due to the differences in acquisition time of enhanced images (30–35 s vs. 23 s; 55–60 s vs. 50 s). They also showed that there were differences in tumor size which agreed with our results.

Subsequently, we compared the texture parameters among G1, G2, and PNEC G3. Our data showed that mean grey-level intensity at three sigma values had great potential for differentiating PNET G1 from PNET G2 with high sensitivity and specificity (both > 0.9). Mean grey-level, entropy, and uniformity also showed acceptable sensitivity (0.73–0.91) and specificity (0.85–1.0) in differentiating PNEC G3 from PNETs G1/G2. Our data indicate that texture analysis is useful for PNENs grading. Canellas et al. [24] indicated that there were differences in mean, mean positive pixels, and entropy between PNET G1 and PNET G2/PNEC. Significant differences in mean grey-level and entropy were also observed in our study. They reported that entropy was the only texture parameter in differentiating PNETs G1 from PNET G2/PNEC [24] by using a regression model. Choi et al. [25] also showed that CT texture variables such as lower sphericity, higher skewness, and lower kurtosis were useful for predicting PNET G2/PNEC. Those studies also indicated that texture analysis is predictive of PNET grades [24, 25]. However, both the two studies did not show the differences between PNET G1/G2 and PNEC because only 3–5 cases of PNEC were included in their study. One study also showed that histogram analysis on MRI ADC map was valuable in grading PNENs [23]. They demonstrated that there were significant differences in skewness and kurtosis between PNET G1 and PNEC G3. In our study, no difference in skewness was found among G1, G2, and G3 tumors, which indicated that texture parameters were associated with imaging modality. In addition, only four cases of PNET G2 and three cases of PNEC G3 were evaluated in that study [23], which may also affect the results. Further studies are needed. Our study is an exploration.

Texture analysis can be performed on unenhanced image or contrast-enhanced image. In the present study, we perform the analysis on arterial enhanced images because PNENs are hyper-vascular tumor. Choi et al. showed that diagnostic performance of texture analysis was better than CT findings [25]. However, only qualitative parameters, such as tumor margin, were assessed in their study. Our data showed that texture parameters were not better than quantitative parameters (including AER and PER). Although the diagnostic performances of texture parameters in differentiating PNEC G3 from PNETs G1/G2 are not better than those traditional indexes, texture analysis is at least an important supple-

ment to radiologists. Moreover, texture analysis shows great advantage in differentiating PNET G1 from PNET G2.

The higher standard deviations in texture parameters were present in PNET G2 and PNEC. PNET G2 and PNEC showed more heterogeneous than PNET G1 on contrast-enhanced imaging [12]. PNET G2 usually showed marked enhancement. Mild enhancement was also found in PNETs G2. PNEC usually showed mild enhancement. However, marked enhancement also can be found in PNEC. Therefore, the standard deviation is higher in PNET G2/PNEC than PNET G1.

Time cost should be considered in texture analysis. The physician takes only several minutes to segment the tumor and draw the ROI, and then the texture data are calculated automatically. However, for larger tumors and whole tumor analysis, the physician may spend much more time than the small one.

Imaging parameters are associated with texture analysis [30]. In our study, tube current may vary individually because automatic tube current modulation was applied. Previous study indicated that texture analysis was sensitive to tube voltage but did not depend on tube current [31]. Slice thickness is another factor that affects texture analysis [32]. The thickness ≤ 3 mm is recommended in texture analysis [32]. In our study, 3 mm of thickness was used. In addition, other imaging parameters are same among patients in our study. Thus, the influence of imaging parameters on texture analysis may be minimal in our study.

There are several limitations in our study. First, PNEC G3 is usually misdiagnosed with pancreatic ductal adenocarcinoma. Many PNEC G3 patients admitted to our institution for further treatment. Patients with PNETs G1/G2 are usually correctly diagnosed and underwent operation in other institutions. The selection bias is unavoidable, and it is not appropriate to calculate the proportion of PNEC G3 based on our study. Second, the sample size is relatively small because of the rarity of PNENs. Further studies with larger sample sizes are needed. Third, we only show the texture features of PNENs on arterial phase images and only a few texture parameters are observed. The features on unenhanced and portal phase images are not investigated. Another limitation is that ROI segmentations are made in consensus by the two readers; we only evaluate the ROI agreement between the readers. In addition, the texture analysis is not performed on the whole tumor. Finally, the PNENs grading is not based on the new WHO 2017 classification of PNENs.

In conclusion, our data indicate that tumor size, pancreatic duct dilation, local invasion/metastases, AER, and PER have potential for differentiating PNEC G3 from PNET G1/G2. Moreover, our data indicate that texture analysis on contrast-enhanced CT images may represent as promising, non-invasive biomarkers to evaluate the pathologic grade of PNENs.

Compliance with ethical standards

Funding This study was supported by the Zhejiang Medical Science and Technology Project (2017KY331) and Primary Research & Development Plan of Jiangsu Province (BE2017772).

Disclosures The authors do not have any possible conflicts of interest.

Ethical approval This retrospective study was approved by the Institutional Review Board of the First Affiliated Hospital, College of Medicine Zhejiang University. For this retrospective study, the requirement of the formal consent was waived.

References

1. Wang Y, Miller FH, Chen ZE, et al. (2011) Diffusion-weighted MR imaging of solid and cystic lesions of the pancreas. Radiographics 31(3):E47–E64
2. Dasari A, Shen C, Halperin D, et al. (2017) Trends in the incidence, prevalence, and survival outcomes in patients with neuroendocrine tumors in the United States. JAMA Oncol 3:1335–1342
3. Klimstra DS, Arnold R, Capella C (2010) Neuroendocrine neoplasms of the pancreas. In: Bosman FT, Carneiro F, Hruban RH, Theise ND (eds) *WHO Classification of Tumours of the Digestive System*. Lyon: International Agency for Research on Cancer (IARC), pp 322–326
4. Kulke MH, Shah MH, Benson Al B, et al. (2014) NCCN guidelines Neuroendocrine tumors version 2. Accessed March.
5. Burns WR, Edil BH (2012) Neuroendocrine pancreatic tumors: guidelines for management and update. Curr Treat Options Oncol 13(1):24–34
6. Yao JC, Shah MH, Ito T, et al. (2011) RAD001 in Advanced Neuroendocrine Tumors, Third Trial (RADIANT-3) Study Group. Everolimus for advanced pancreatic neuroendocrine tumors. N Engl J Med 364(6):514–523
7. Raymond E, Dahan L, Raoul JL, et al. (2011) Sunitinib malate for the treatment of pancreatic neuroendocrine tumors. N Engl J Med 364(6):501–513
8. Cappelli C, Boggi U, Mazzeo S, et al. (2015) Contrast enhancement pattern on multidetector CT predicts malignancy in pancreatic endocrine tumours. Eur Radiol 25(3):751–759
9. Kim DW, Kim HJ, Kim KW, et al. (2015) Neuroendocrine neoplasms of the pancreas at dynamic enhanced CT: comparison between grade 3 neuroendocrine carcinoma and grade 1/2 neuroendocrine tumour. Eur Radiol 25(5):1375–1383
10. Takumi K, Fukukura Y, Higashi M, et al. (2015) Pancreatic neuroendocrine tumors: Correlation between the contrast-enhanced computed tomography features and the pathological tumor grade. Eur J Radiol 84(8):1436–1443
11. Horiguchi S, Kato H, Shiraha H, et al. (2017) Dynamic computed tomography is useful for prediction of pathological grade in pancreatic neuroendocrine neoplasm. J Gastroenterol Hepatol 32(4):925–931
12. Lotfalizadeh E, Ronot M, Wagner M, et al. (2017) Prediction of pancreatic neuroendocrine tumour grade with MR imaging features: added value of diffusion-weighted imaging. Eur Radiol 27(4):1748–1759
13. Guo C, Chen X, Xiao W, et al. (2017) Pancreatic neuroendocrine neoplasms at magnetic resonance imaging: comparison between grade 3 and grade 1/2 tumors. Onco Targets Ther 10:1465–1474
14. Giganti F, Antunes S, Salerno A, et al. (2017) Gastric cancer: texture analysis from multidetector computed tomography as a potential preoperative prognostic biomarker. Eur Radiol 27(5):1831–1839
15. Aerts HJ, Velazquez ER, Leijenaar RT, et al. (2014) Decoding tumour phenotype by noninvasive imaging using a quantitative radiomics approach. Nat Commun 5:4006
16. Choi ER, Lee HY, Jeong JY, et al. (2016) Quantitative image variables reflect the intratumoral pathologic heterogeneity of lung adenocarcinoma. Oncotarget 7(41):67302–67313

17. Summers RM (2017) Texture analysis in radiology: Does the emperor have no clothes? Abdom Radiol (NY) 42(2):342–345
18. Sacconi B, Anzidei M, Leonardi A, et al. (2017) Analysis of CT features and quantitative texture analysis in patients with lung adenocarcinoma: a correlation with EGFR mutations and survival rates. Clin Radiol 72(6):443–450
19. Ramkumar S, Ranjbar S, Ning S, et al. (2017) MRI-based texture analysis to differentiate sinonasal squamous cell carcinoma from inverted papilloma. AJNR Am J Neuroradiol 38(5):1019–1025
20. Nketiah G, Elschot M, Kim E, et al. (2017) T2-weighted MRI-derived textural features reflect prostate cancer aggressiveness: preliminary results. Eur Radiol 27(7):3050–3059
21. Kim JH, Ko ES, Lim Y, et al. (2017) Breast cancer heterogeneity: MR imaging texture analysis and survival outcomes. Radiology 282(3):665–675
22. Zhang S, Zhang B, Tian J, et al. (2017) Radiomics features of multiparametric MRI as novel prognostic factors in advanced nasopharyngeal carcinoma. Clin Cancer Res 23(15):4259–4269
23. Pereira JA, Rosado E, Bali M, et al. (2015) Pancreatic neuroendocrine tumors: correlation between histogram analysis of apparent diffusion coefficient maps and tumor grade. Abdom Imaging 40(8):3122–3128
24. Canellas R, Burk KS, Parakh A, et al. (2018) Prediction of pancreatic neuroendocrine tumor grade based on CT features and texture analysis. AJR Am J Roentgenol 210(2):341–346
25. Choi TW, Kim JH, Yu MH, et al. (2018) Pancreatic neuroendocrine tumor: prediction of the tumor grade using CT findings and computerized texture analysis. Acta Radiol 59(4):383–392
26. Ganeshan B, Miles KA, Young RC, et al. (2007) Hepatic entropy and uniformity: additional parameters that can potentially increase the effectiveness of contrast enhancementduring abdominal CT. Clin Radiol 62(8):761–768
27. Miles KA, Ganeshan B, Hayball MP (2013) CT texture analysis using the filtration-histogram method: what do the measurements mean? Cancer Imaging 13(3):400–406
28. Goh V, Ganeshan B, Nathan P, et al. (2011) Assessment of response to tyrosine kinase inhibitors in metastatic renal cell cancer: CT texture as a predictive biomarker. Radiology 261(1):165–171
29. Rao SX, Lambregts DM, Schnerr RS, et al. (2014) Whole-liver CT texture analysis in colorectal cancer: Does the presence of liver metastases affect the texture of the remaining liver? United Eur Gastroenterol J 2(6):530–538
30. Li M, Fu S, Zhu Y, et al. (2016) Computed tomography texture analysis to facilitate therapeutic decision making in hepatocellular carcinoma. Oncotarget 7(11):13248–13259
31. Miles KA, Ganeshan B, Griffiths MR, et al. (2009) Colorectal cancer: texture analysis of portal phase hepatic CT images as a potential marker of survival. Radiology 250(2):444–452
32. Guggenbuhl P, Chappard D, Garreau M, et al. (2008) Reproducibility of CT-based bone texture parameters of cancellous calf bone samples: influence of slice thickness. Eur J Radiol 67(3):514–520